Crystal structure, photoluminescence and cathodoluminescence of Ba$_{1-x}$Sr$_x$Al$_2$O$_4$ doped with Eu^{2+}

MAX VOLHARD,[2] LIPING YU,[3] DANIEL DEN ENGELSEN,[1] GEORGE R. FERN,[1] TERRY G. IRELAND,[1] AND JACK SILVER[1,*]

[1] *Centre for Phosphor and Display Materials, Wolfson Centre for Materials Processing, Brunel University London, Uxbridge, Middlesex, UB8 3PH, UK*

[2] *On leave from Department of Chemical Engineering, Münster University of Applied Sciences, Stegerwaldstrasse, 39, Steinfurt, D-48565, Germany*

[3] *On leave from the College of Chemistry and Chemical Engineering, Hunan Normal University, Changsha, 410081, China*

[*] *jack.silver@brunel.ac.uk*

Abstract: Herein we describe the synthesis, crystal structures, photoluminescence (PL) and cathodoluminescence (CL) spectra of phosphors in the Sr$_{0.97-x}$Ba$_x$Eu$_{0.03}$Al$_2$O$_4$ system between x = 0 and x = 0.97. The syntheses of these phosphors were carried out by solid state reactions at 1350°C in mixed gas (H$_2$/N$_2$). The molar fractions of the alkaline earth elements were varied in steps of 0.1. The Sr$_{1-x}$Ba$_x$Al$_2$O$_4$ series manifested solid solutions of a monoclinic phase (at the Sr-rich side) and a hexagonal phase (at the Ba-rich side). At the Ba-rich side of Sr$_{x-1}$Ba$_x$Al$_2$O$_4$:Eu^{2+} we found evidence in the PL spectra that the hexagonal phase differed as the x$_{Ba}$ fraction changed: it changed at room temperature from the ferroelectric P6$_3$ structure at x$_{Ba}$=1 to the paraelectric P6$_3$22 phase at x$_{Ba}$≈0.9 and at x$_{Ba}$≈0.8 it went back to P6$_3$. Unlike the PL spectra, the CL spectra of the hexagonal phase of Sr$_{0.97-x}$Ba$_x$Eu$_{0.03}$Al$_2$O$_4$ at x ≥ 0.5 indicated only the paraelectric P6$_3$22 phase at room temperature.

1. Introduction

This article is the second part of an ongoing study on the phosphor series Ba$_{1-x}$Sr$_x$Al$_2$O$_4$, Sr$_{1-x}$Ca$_x$Al$_2$O$_4$ and Ba$_{1-x}$Ca$_x$Al$_2$O$_4$ doped with Eu^{2+}. In [1] we have described the crystal structures and luminescence of phosphors in the Sr$_{1-x}$Ca$_x$Al$_2$O$_4$:Eu^{2+} series of materials. Herein we shall describe the results for Ba$_{1-x}$Sr$_x$Al$_2$O$_4$:Eu^{2+}, while the results for Ba$_{1-x}$Ca$_x$Al$_2$O$_4$ will be published separately. We have presented a general introduction to the structure and luminescence of alkaline earth aluminates doped with Eu^{2+} in reference [1] and we refer to this for the motivation of this research.

SrAl$_2$O$_4$ has a monoclinic crystal structure at ambient temperature and pressure [1], the hexagonal structure is the stable phase at a temperature > 675°C, then it is again monoclinic at even higher temperatures [2,3]. BaAl$_2$O$_4$ has a hexagonal structure at 25°C [4]; it attracted special attention due to its phase change from the ferroelectric (space group P6$_3$) to the paraelectric state (space group P6$_3$22), which takes place at 400 K-450 K [5,6].

Fig. 1 presents the composition diagram of the ternary system BaO-SrO-Al$_2$O$_3$, which is largely based on the data presented in Shuklás thesis [7], the literature mentioned therein and the work of Ptáček [8] and Ropp [9]. In Fig. 1 the notation of the cement chemistry has been adopted, in which A stands for Al$_2$O$_3$, B stands for BaO and S stands for SrO. These abbreviations will also be used in this paper. The red line BA-SA indicates the compositions that were investigated

and are described herein. The compounds in Fig. 1 emphasized with a red mark that are not positioned on the red line could be present as a byproduct of the all-solid state reactions, carried out in the this investigation.
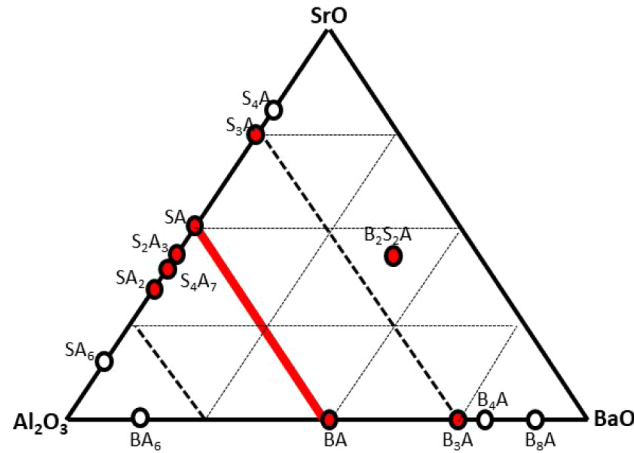
Fig. 1. Composition diagram of BaO-SrO-Al_2O_3. The cement chemistry notation has been adopted to denote the compounds in this ternary system. The red line indicates the compositions that were studied.

The stable compounds in the vicinity of the line BA-SA in Fig. 1 at 1350°C are: B_2S_2A (di-barium di-strontium aluminate), B_3A (tri-barium aluminate), S_3A (tri-strontium aluminate), S_2A_3 (di-strontium tri-aluminate), S_4A_7 (tetra-strontium hepta-aluminate) and SA_2 (strontium di-aluminate). We shall focus on only a limited part of the ternary system of B-S-A, namely on the compounds formed on the line BA-SA ($Sr_{1-x}Ba_xAl_2O_4$, abbreviated BSA) in B-S-A. The crystal phases in BSA were studied by Rodehorst et al. [10] using electron diffraction and infrared spectroscopy: they found ferroelectric hexagonal BSA at the Ba-rich side and monoclinic BSA at the Sr-rich side. Kawaguchi et al. [11] and Tanaka et al. [12] found that partially substituting Sr^{2+} for Ba^{2+} in $BaAl_2O_4$ suppressed the ferroelectric phase with space group $P6_3$ in $Ba_{0.9}Sr_{0.1}Al_2O_4$. These results indicated that the temperature of the phase transition decreased appreciably from about $450\,K$ for pure $BaAl_2O_4$ to around $300\,K$ by introducing only a small quantity of Sr. Rezende et al. [13] observed Eu^{2+} and Eu^{3+} peaks in the X-ray excited spectra of BSA doped with Eu^{2+}. However, their samples were annealed in air and not in a reducing atmosphere. Blasse and Bril [14] mentioned that in $Sr_{1-x}Ba_xAl_2O_4:Eu^{2+}$ the emission band showed a blue shift upon increasing the Ba content. More details were published by Poort et al. [15], Ryu et al. [16] on $Sr_{1-x}Ba_xAl_2O_4:Eu^{2+}$ and Xie et al. [17] on the PL spectra of $Sr_{1-x}Ba_xAl_2O_4:Eu^{2+},Dy^{3+}$. The latter authors measured minimum PL at $x_{Ba}=0.45$, which is the boundary between the hexagonal and monoclinic phases in the phase diagram of $Sr_{1-x}Ba_xAl_2O_4$ [10].

As part of the study on (Ba, Ca, Sr)Al_2O_4:Eu aluminates we describe the results of the XRD and spectroscopic investigations of the $Sr_{1-x}Ba_xAl_2O_4$:Eu series in this article. Detailed results for $BaAl_2O_4:Eu^{2+}$ will be described in the forthcoming articles on $Ba_{1-x}Ca_xAl_2O_4:Eu^{2+}$ and $BaAl_2O_4:Eu^{2+}$.

2. Experimental

2.1. Materials

Starting materials were: strontium carbonate (Sigma Aldrich, UK, 99.9%), barium carbonate (Alfa Aesar, UK, 99%), aluminum oxide (SASOL Inc., USA), europium oxide (Ampere Industrie,

France, 99.99%), and concentrated hydrochloric acid (Sigma Aldrich, UK, 37%). All materials were used as supplied without further purification. The final annealing of the powders was made in Al_2O_3 crucibles at high temperatures in H_2 (10%)/N_2 (90%) gas.

2.2. Synthesis

Solid state synthesis methods were used to prepare $Sr_{1-y-x}Eu_yBa_xAl_2O_4$ with x varying between 0 and 0.99 or 0.97 in steps of 0.1 and y = 0.01 and 0.03. The samples were prepared by calcining mixtures of an appropriate molar ratio of $SrCO_3$, $BaCO_3$, γ-Al_2O_3 and $EuCl_3$ powders in a flow of 90% N_2–10% H_2. After calcination the powders were carefully ground by ball milling (Al_2O_3) for 3 hours. The final annealing of the $Sr_{1-y-x}Eu_yBa_xAl_2O_4$ samples was made at 1350°C. PL spectra and X-ray diffraction (XRD) spectra were recorded a few days after synthesizing the phosphors. CL spectra of some samples were recorded at 200 keV electron beam energy after 4 years of shelf life at ambient conditions.

2.3. Characterization

The characterization equipment, X-ray diffractometer (XRD) and transmission electron microscope (TEM), has been described in detail in part 1 [1]. Crystalline phases in the prepared samples were identified from the XRD-patterns by peak-search matching using the ICCD PDF-2 data files. The identifiable phases were refined according to the Rietveld procedures using the Topas package. The fundamental parameters approach was used. For the morphology and particle size assessment of the phosphor powders we also used a field emission scanning electron microscope (FESEM): Supra 35 VP, Carl Zeiss, Germany. PL excitation and emission spectra of the samples were recorded using a Bentham spectrometer system (Bentham Instruments Ltd., Reading, UK.), configured with M300 excitation and emission monochromators, which were equipped with 0.2 mm slits. The wavelength scale of the monochromators had a maximum error of ~0.4 nm.

3. Results and discussion

3.1. Electron microscope

The particle size of the alkaline earth aluminates after the high temperature annealing process was in all cases rather large and varied from about 1 to 6 μm. Figs. 2(a) and 2(b) are SEM images of samples after the final annealing step.
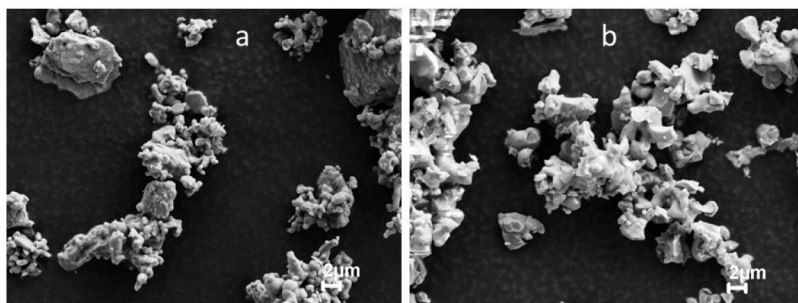

Fig. 2. (a) SEM image at 7 keV of $BaAl_2O_4$:3%Eu^{2+} annealed at 1350°C. (b) SEM image at 7 keV of $Sr_{0.37}Ba_{0.6}Al_2O_4$:3%Eu^{2+}.

Figs. 2(a) and 2(b) manifest that crystallites sinter and form agglomerates. At temperatures >1400°C there is more sintering and the agglomerates grow in size. For this reason we have limited the annealing temperature to 1350°C.

3.2. X-ray diffraction and crystal structure

Figs. 3(a) and (b) present powder XRD patterns of $Sr_{0.99-x}Ba_xEu_{0.01}Al_2O_4$ ($0 \leq x \leq 0.99$).

In the $Ba_{0.97-x}Sr_xEu_{0.03}Al_2O_4$ (and $Ba_{0.99-x}Sr_xEu_{0.01}Al_2O_4$) series we found only two phases, viz. the hexagonal $BaAl_2O_4$ phase (BA) with space group $P6_3$ and the monoclinic $SrAl_2O_4$ phase (MCSr) with space group $P2_1$. The lattice parameters of these two phases are indicated in Tables 1 and 2 respectively in the appendix. These phosphor series behave rather ideally: from $0 < x \leq 0.6$ we have 100% solid solution of hexagonal BA and from $0.6 < x < 1$ we have a 100% solid solution of MCSr. This behaviour is illustrated in Fig. 4, which is a Vegard plot of the volumes of the hexagonal and monoclinic cells of this phosphor series. This result agrees with the findings of Rodehorst et al. [10]. The latter scientists and Kawaguchi et al. [11] found a phase transition in hexagonal BSA at the Ba-rich side ($x > 0.1$) from $P6_3(2A) \rightarrow P6_3(\sqrt{3}A)$ [10] or $P6_3(2A) \rightarrow P6_322(A)$ [12]. It was impossible to confirm this result from the XRD pattern in Fig. 3(a); however, we found evidence for this transition by analysing the PL spectra, to be described in the next section.
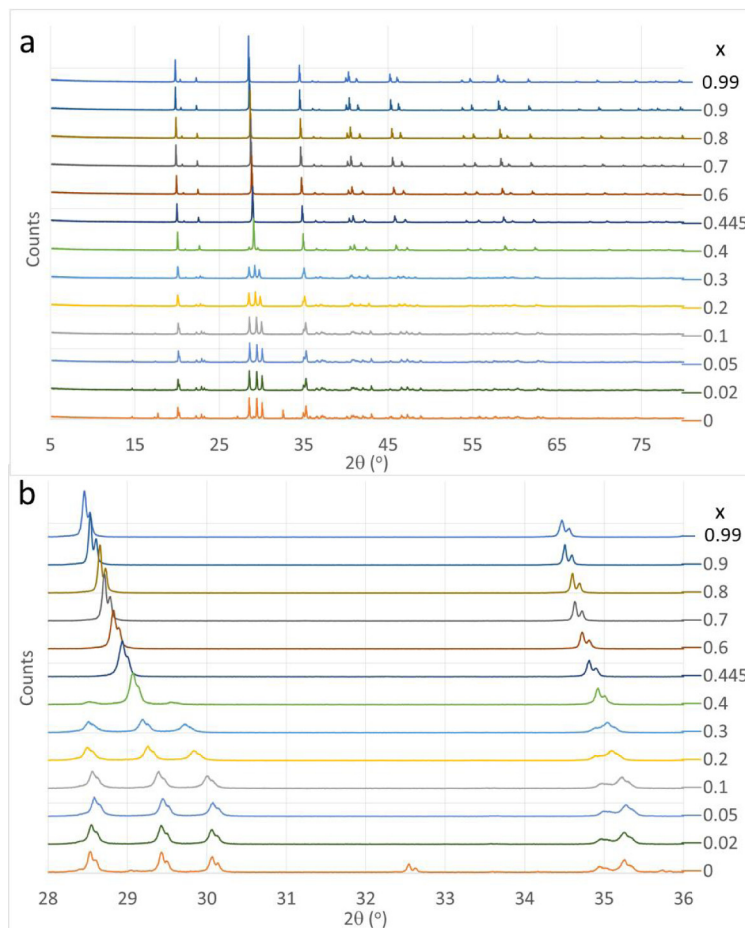
Fig. 3. Powder XRD patterns of $Sr_{0.99-x}Ba_xEu_{0.01}Al_2O_4$ for $0 \leq x \leq 0.99$. (a) $5° \leq 2\theta \leq 80°$. (b) Enlarged pattern for the range $28° \leq 2\theta \leq 36°$.

The straight lines that are fitted to the data points presented in Fig. 4 coincide nicely for the series with 1 and 3 mol % Eu^{2+}.
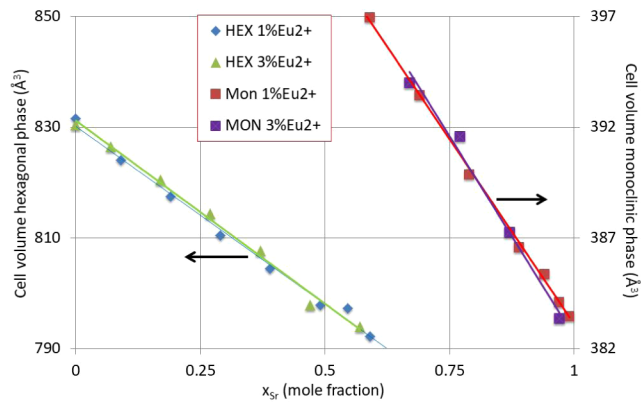
Fig. 4. Vegard plot of the cell volumes of the hexagonal BA phase and MCSr in $Ba_{0.97-x}Sr_xEu_{0.03}Al_2O_4$ and $Ba_{0.99-x}Sr_xEu_{0.01}Al_2O_4$. The straight lines have been fitted to the experimental data points.

3.3.   PL and CL spectra

In Fig. 5 the PL spectra of the phosphor series $Sr_{0.97-x}Ba_xAl_2O_4$:3%Eu^{2+} have been plotted for various values of the molar fraction of Ba^{2+}. The PL spectra illustrated in Figs. 5(a) and 5(b) agree nicely with the spectra published by Xie et al. [17] for $Sr_{0.9-x}Ba_xEu_{0.05}Dy_{0.05}Al_2O_4$. The maximum spectral radiance has the lowest value at x_{Ba}=0.37: the spectra of the single alkaline earth aluminates have higher spectral radiances than aluminates with two alkaline earth ions. A common feature of the emission spectra in Fig. 5(a) is the asymmetric shape of the main emission bands, viz. the bands show a tail at the long wavelength side. This is even the case in a wavenumber or energy representation of the spectra, which reduces the asymmetry slightly. The PL spectra of $Sr_{1-x}Ca_xAl_2O_4$:Eu^{2+} (CSA) published in [1] feature broadening of the emission band at mole fractions between 0.4 and 0.6, whereas Fig. 5(a), does not show broadening of the band at $0.2 < x < 0.8$. In the BSA system solid solutions are formed, which imply that at a certain molar fraction of Ba only one phase, either having the monoclinic or the hexagonal structure, can be present in the sample. This is different in the other phosphor systems: in CSA we have at $0.2 < x_{Ca} < 0.5$ three different phases in sufficiently high concentrations, as indicated in [1]. These different phases have different crystal structures and create different electrostatic environments for the Eu^{2+} ions, which leads to band broadening. In the PL spectra of $Sr_{0.99-x}Ca_xEu_{0.01}Al_2O_4$ published in part 1 [1] we found an emission band at 440 nm when a small quantity of Ca was added to $SrAl_2O_4$:Eu^{2+}. Due to the presence of a small quantity of the monoclinic $P2_1/n$ phase in $Sr_{1-x}Ca_xAl_2O_4$:Eu^{2+} with a small molar fraction of Ca this band was assigned to the 440 nm emission band of $CaAl_2O_4$ at room temperature. In the PL spectra of $Sr_{1-x}Ba_xAl_2O_4$:Eu^{2+} no sign of an additional emission band was found when (small amounts of) Ba was added to $SrAl_2O_4$:Eu^{2+}.

From the temperature dependence of the PL spectra Poort et al. [15] determined the quenching temperatures T_q of some $Sr_{1-x}Ba_xAl_2O_4$:Eu^{2+} compounds. Fig. 6 is a comparison of results.

For $SrAl_2O_4$:Eu we found a much lower quenching temperature than Poort et al. [15]. From the data published by Botterman et al. [18] and Ueda et al. [19] T_q of $SrAl_2O_4$:Eu,Dy can be estimated to be about 500 K.

Fig. 7 is a collection of diagrams that show deconvolutions of PL spectra of the BSA-series at the Ba-side recorded at room temperature. The fitting of the deconvoluted spectrum to the experimental spectrum was carried out using Gaussian profiles and a least squares algorithm in a wavenumber (cm^{-1}) representation as described previously [1,20,21]. In the deconvolutions we
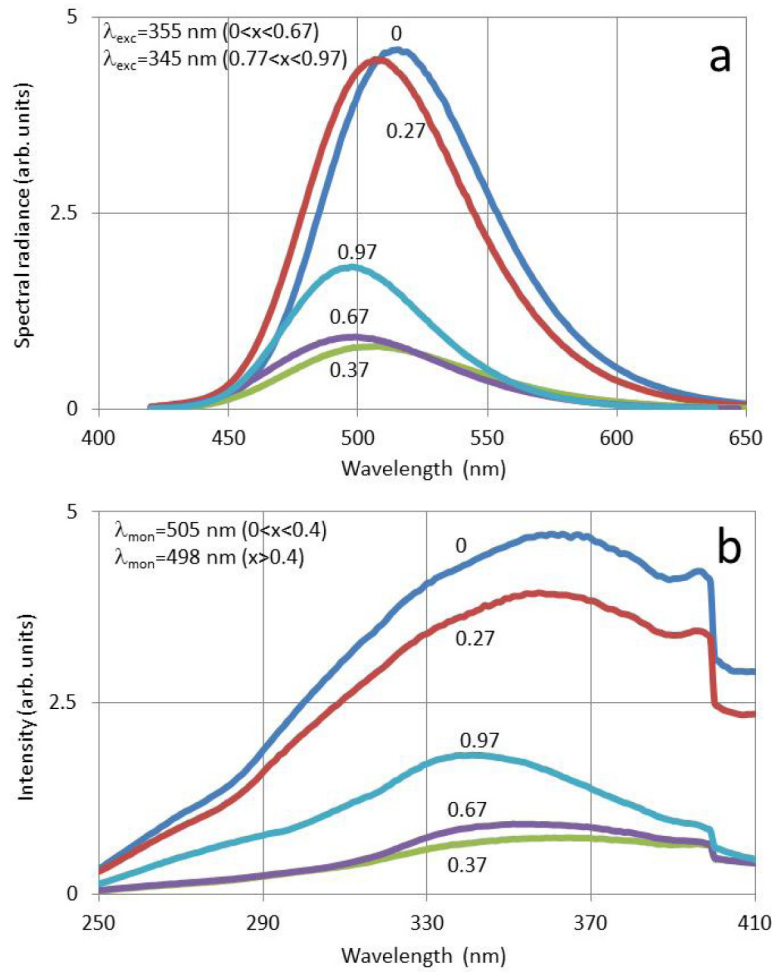
Fig. 5. Photoluminescence spectra of $Sr_{0.97-x}Ba_xAl_2O_4{:}3\%Eu^{2+}$ at various values of x_{Ba}. (a) Emission spectra. (b) Excitation spectra. For clarity reasons only a limited number of spectra are shown. The kink at 400 nm in the excitation spectra is due to a filter change of the spectrometer.
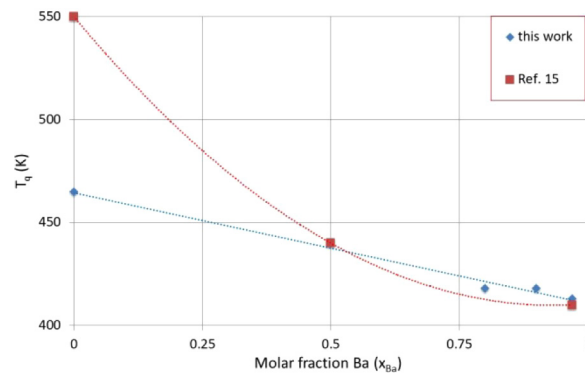
Fig. 6. Quenching temperature T_q versus mole fraction of Ba in $Sr_{0.97-x}Ba_xEu_{0.03}Al_2O_4$. Curves have been fitted to the experimental data.

have taken the minimum number of profiles that gave a good fit with the experimental spectra. The radiance R of a Gaussian profile is the area under the curve. λ_0 is the wavelength at maximum spectral radiance for a profile and ν_0 is the corresponding wavenumber.
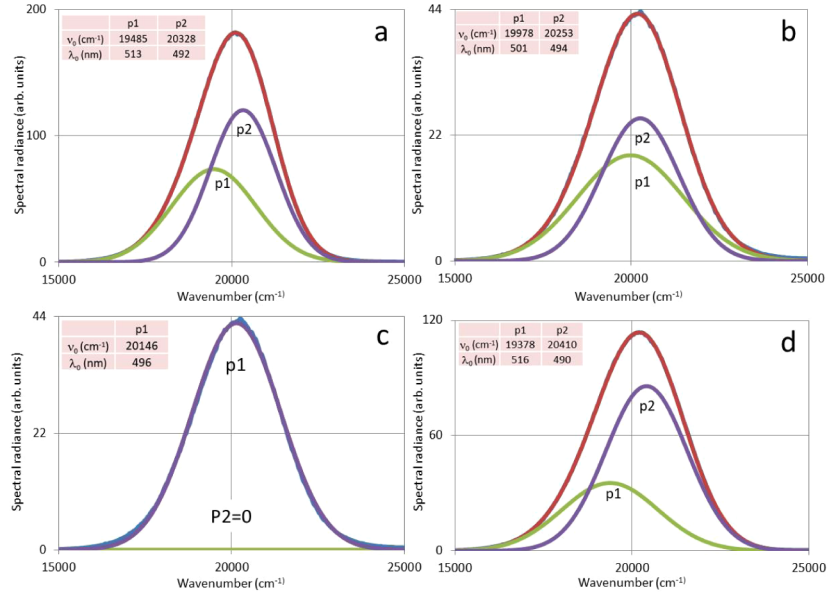

Fig. 7. Deconvolution of PL spectra of $Sr_{0.97-x}Ba_xAl_2O_4$:3%Eu^{2+} with two (or one) Gaussian profiles. (a) $Ba_{0.97}Eu_{0.03}Al_2O_4$, exc.: 341 nm. (b) $Sr_{0.07}Ba_{0.9}Eu_{0.03}Al_2O_4$, exc.: 345 nm. (c) $Sr_{0.07}Ba_{0.9}Eu_{0.03}Al_2O_4$, exc.: 345 nm, deconvoluted with only one Gaussian profile. (d) $Sr_{0.17}Ba_{0.8}Eu_{0.03}Al_2O_4$, exc.: 355 nm.

The emission bands in Fig. 7 are asymmetric and can be well rendered by two Gaussian profiles. However, the emission band of $Sr_{0.07}Ba_{0.90}Eu_{0.03}Al_2O_4$ in Fig. 7(b) is less asymmetric and can adequately be described by only one Gaussian profile; this is shown in Fig. 7(c). The spectra of the other samples of this series cannot accurately be represented with one Gaussian profile. In Figs. 8(a) and 8(b) we have plotted ν_0 and the full width at half maximum (FWHM) respectively of the two profiles p1 and p2 profiles versus x_{Ba}.

The data shown in Figs. 7 and 8 indicate that the spectrum of $Sr_{0.07}Ba_{0.9}Eu_{0.03}Al_2O_4$ deviates from the others, since the asymmetry of its emission band, expressed as the difference $\nu_0(p2)$ - $\nu_0(p1)$ in Fig. 8(a), is much smaller than it is for the other spectra. Although $\nu_0(p2)$ - $\nu_0(p1)$ does not go to 0 cm^{-1} for the sample at x_{Ba}=0.9, it is apparent that the residual asymmetry, which could be caused by the presence of two phases or electron-phonon coupling, is small. This leads to the assumption that the emission band of the $Sr_{0.07}Ba_{0.9}Eu_{0.03}Al_2O_4$ sample may be rendered by one Gaussian profile, as shown in Figs. 7(c) and 8(b). The FWHM of the single profile for this sample is equal to the FWHM of the p1 profile. If the luminescence of a phosphor doped with Eu^{2+} can be represented by one Gaussian profile, then two possibilities need to be considered: (1) there may be more than one cation site, but only one is occupied by Eu^{2+}; (2) there is only one cation site present in the lattice. When ferroelectric $BaAl_2O_4$ with space group $P6_3$ changes into the paraelectric phase with space group $P6_322$, the volume of the unit cell becomes four times smaller and the number of different alkaline earth cation sites reduces from 2 to 1. In $BaAl_2O_4$:Eu^{2+} without any Sr addition (see Fig. 7(a)) it is apparent that two Gaussian profiles are needed to represent the spectrum: these profiles refer to the Eu^{2+} ions at the two Ba sites. By introducing a small quantity of Sr there is no reason why the Eu^{2+} ions should migrate to only one Ba site. Hence, it is assumed here that $Sr_{0.07}Ba_{0.90}Eu_{0.03}Al_2O_4$ has the high symmetry space

group $P6_3 22$ with only one unique Ba site. For the other mole fractions of Ba the hexagonal phase of BSA has the ferroelectric $P6_3$ phase. It is therefore concluded that the data in Fig. 7 are an indication that the hexagonal phase of BSA changes from the ferroelectric $P6_3$ structure at $x_{Ba}=1$ to the paraelectric $P6_3 22$ phase at $x_{Ba} \approx 0.9$ and at $x_{Ba} \approx 0.8$ it goes back to $P6_3$.
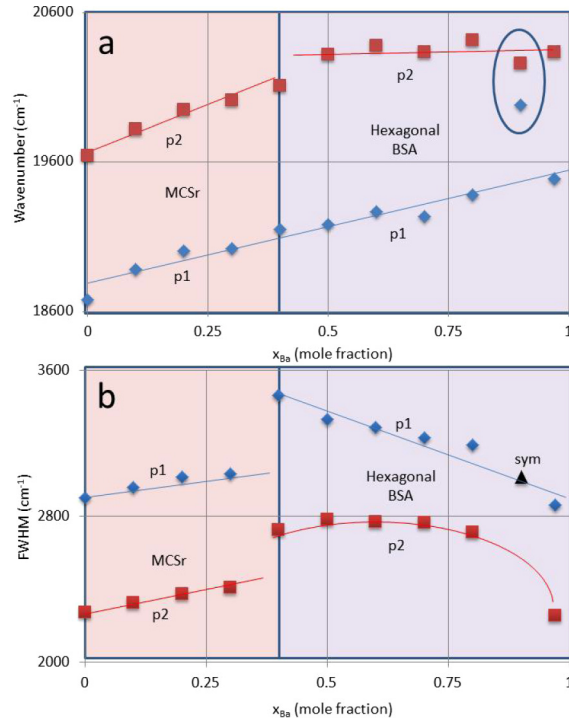
Fig. 8. (a) ν_0 of the two profiles p1 and p2 versus x_{Ba} of the BSA series. The values at $x_{Ba}=0.9$ cannot be considered to be outliers, since all deconvolutions were performed with more than 200 data points. (b) FWHM of p1 and p2 versus x_{Ba}. The data indicate clearly the phase transition at $x_{Ba} \approx 0.4$.

In Fig. 9 some CL spectra of $Sr_{0.07}Ba_{0.9}Eu_{0.03}Al_2O_4$ and $Sr_{0.27}Ba_{0.7}Eu_{0.03}Al_2O_4$ are presented. It is apparent that under Cl excitation that there is clear evidence of Eu^{3+} in the spectra in Fig. 9. As mentioned in section 2.2, these spectra were recorded after 4 years of shelf life at ambient conditions. Compared to the amount of the Eu^{2+} emission present in the spectra, the Eu^{3+} emission is small and is not further covered herein as it is treated as an oxidation contaminant. It should be noted however that the Eu^{3+} emission bands differ in the two samples possibly providing evidence that the lattice sites it occupies in the two materials have different symmetries. Indeed this finding does fit with the findings for the Eu^{2+} emission bands which are discussed in detail below.

Figs. 9(a) and 9(c) indicate that $Sr_{0.27}Ba_{0.7}Eu_{0.03}Al_2O_4$ and $Sr_{0.07}Ba_{0.9}Eu_{0.03}Al_2O_4$ yield completely different CL spectra upon lowering the temperature. The low temperature CL spectrum of $Sr_{0.07}Ba_{0.9}Eu_{0.03}Al_2O_4$ is similar to that of $BaAl_2O_4$:Eu without any Sr. The peak at about 410 nm is ascribed herein to an F-centre; this interesting behaviour will be described in detail in a forthcoming publication. Figs. 9(b) and 9(d) present deconvolutions of the room temperature spectra shown in Figs. 9(a) and 9(c) respectively. Unlike the PL spectra of $Sr_{0.97-x}Ba_xEu_{0.03}Al_2O_4$ at $x < 0.9$, the CL spectra can be represented by one Gaussian profile, which means that as soon as Sr has been added to BA, the hexagonal paraelectric phase is more stable than the ferroelectric phase. The insert of Fig. 9(a) is an Arrhenius plot of the maximum
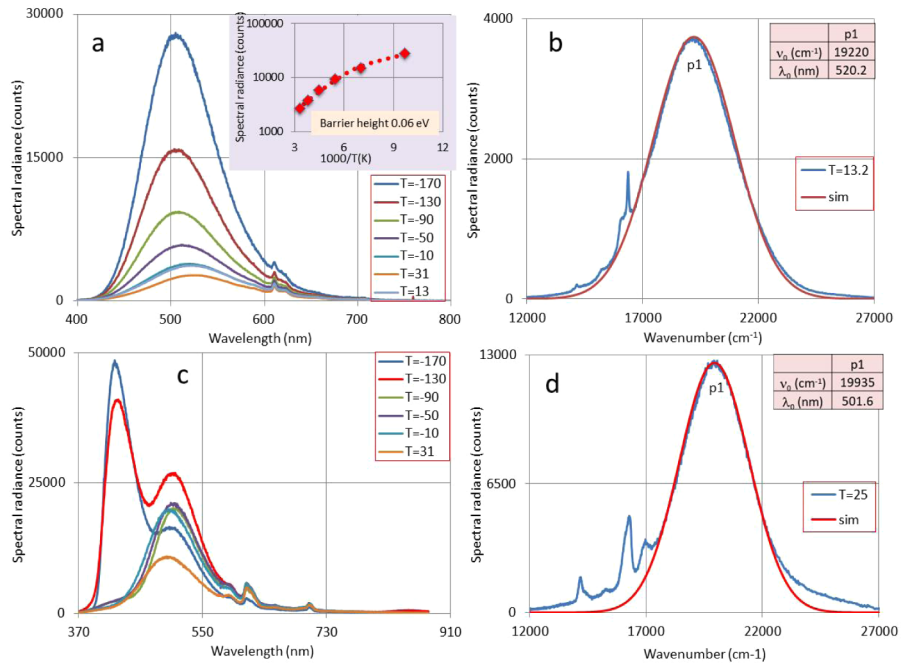
Fig. 9. (a) CL spectra of $Sr_{0.27}Ba_{0.7}Eu_{0.03}Al_2O_4$ recorded at 200 keV and various temperatures. The insert is an Arrhenius plot of the maximum spectral radiance. (b) Deconvolution with one Gaussian profile of the CL spectrum of $Sr_{0.27}Ba_{0.7}Eu_{0.03}Al_2O_4$ recorded at 13°C. (c) CL spectra of $Sr_{0.07}Ba_{0.9}Eu_{0.03}Al_2O_4$ recorded at 200 keV and various temperatures. (d) Deconvolution with one Gaussian profile of the CL spectrum of $Sr_{0.07}Ba_{09}Eu_{0.03}Al_2O_4$ recorded at 25°C.

spectral radiance. The curve is a Fermi-Dirac type fitting to the experimental data [22]. The single-barrier height is 0.06 eV.

The suppression of the ferroelectric $P6_3$ phase of $BaAl_2O_4$ by introducing a small quantity of Sr has been reported by Kawaguchi et al. [11] and Tanaka et al. [12]. They based their findings on XRD-investigations at low (and high) temperatures. They also found that the paraelectric $P6_322$ phase returns to the ferroelectric $P6_3$ phase upon increasing the mole fraction of Sr^{2+} above 0.1. The analysis of the PL spectrum with 7 mol% Sr presented herein matches favourably with their findings. Rodehorst et al. [10] also found that the $P6_3 \rightarrow P6_322$ transition in $BaAl_2O_4$ takes place at temperatures much lower than 450 K by adding a small amount of Sr. The different behaviour of $Sr_{0.97-x}Ba_xEu_{0.03}Al_2O_4$ upon excitation with UV or electron beam may be caused by the excitation energy. In the case of CL the crystals are bombarded with 200 keV electrons, which are supposed to facilitate the transition from the ferroelectric phase to the paraelectric phase at room temperature.

Unlike the excitation spectrum of $Sr_{0.99-x}Ca_xAl_2O_4:1\%Eu^{2+}$ described in [1], the excitation spectra of $Sr_{0.97-x}Ba_xAl_2O_4:3\%Eu^{2+}$ presented in Fig. 5(b) do not present much structure. Moreover the kink at 400 nm makes the spectra less inappropriate for detailed analyses.

4. Conclusion

Apart from a confirmation of forming solid solutions of hexagonal BSA and monoclinic BSA in the series $Sr_{0.97-x}Ba_xEu_{0.03}Al_2O_4$, we have presented evidence for phase transitions in hexagonal BSA as a function of the Ba molar fraction. At $x_{Ba}=0.97$ we have the ferroelectric $P6_3$ phase,

which changes to the paraelectric $P6_322$ phase at $x_{Ba} \approx 0.9$ and at $x_{Ba} \approx 0.8$ it goes back to $P6_3$. These phase transitions take place at room temperature. This conclusion is based on the deconvolution of the PL spectra. Upon excitation with high energy electrons we only detected the paraelectric phase of hexagonal $Sr_{0.97-x}Ba_xEu_{0.03}Al_2O_4$.

Appendix

Table 1. Hexagonal BA in $Ba_{0.97-x}Sr_xEu_{0.03}Al_2O_4$

Sr content (mole fraction)	Composition (%)	Unit cell parameters		
		a (Å)	c (Å)	V(Å^3)
0	100	10.44524	8.78843	830.4
0.07	100	10.43684	8.76085	826.4
0.17	100	10.42136	8.7237	820.5
0.27	100	10.4032	8.68851	814.3
0.37	100	10.38286	8.65152	807.7
0.47	100	10.34696	8.60604	797.9
0.57	100	10.33986	8.57518	794.0
0.67	0			

Table 2. Monoclinic SA in $Ba_{0.97-x}Sr_xEu_{0.03}Al_2O_4$

Sr content (mole fraction)	Composition (%)	Unit cell parameters				
		a (Å)	b(Å)	c (Å)	β (°)	V(Å^3)
0.57	0	n.a.	n.a.	n.a.	n.a.	n.a.
0.67	100	8.55486	8.912	5.17312	92.5934	394.0
0.77	100	8.51958	8.88523	5.17974	92.898	391.6
0.87	100	8.48047	8.85411	5.16548	93.1698	387.3
0.97	100	8.44162	8.82158	5.15698	93.4019	383.4

References

1. L. Yu, D. den Engelsen, J. Gorobez, G. R. Fern, T. G. Ireland, C. Frampton, and J. Silver, "Crystal structure, photoluminescence and cathodoluminescence of $Sr_{1-x}Ca_xAl_2O_4$ doped with Eu^{2+}," Opt. Mater. Express **9**(5), 2175–2195 (2019).
2. A.-R. Schulze and H. Müller-Buschbaum, "Compound Formation MeO:M_2O_3. IV. Structure of Monoclinic $SrAl_2O_4$," Z. Anorg. Allg. Chem. **475**(4), 205–210 (1981).

3. M. Avdeev, S. Yakovlev, A. A. Yaremchenko, and V. V. Kharton, "Transitions between $P2_1$, $P6_3(\sqrt{3}A)$, and $P6_32$ modifications of $SrAl_2O_4$ by in situ high-temperature X-ray and neutron diffraction," J. Solid State Chem. **180**(12), 3535–3544 (2007).
4. W. Hörkner and H. Müller-Buschbaum, "About the crystal structure of $BaAl_2O_4$," Z. Anorg. Allg. Chem. **451**(1), 40–44 (1979).
5. S. Y. Huang, R. Von Der Muehll, J. Ravez, and M. Couzi, "Phase transition and symmetry in $BaAl_2O_4$," Ferroelectrics **159**(1), 127–132 (1994).
6. A. M. Abakumov, O. I. Lebedev, L. Nistor, G. Van Tendeloo, and S. Amelinkx, "The ferroelectric phase transition in tridymite type $BaAL_2O_4$ studied by electron microscopy," Phase Transitions **71**(2), 143–160 (2000).
7. A. Shukla, "Development of a critically evaluated thermodynamic database for the systems containing alkaline-earth oxides," Thesis, University of Montreal, (2012).
8. P. Ptáček, *Strontium Aluminate - Cement Fundamentals, Manufacturing, Hydration, Setting Behaviour and Application*, (InTech, 2014), Chapter 1.
9. R. C. Ropp, *Encyclopedia of the Alkaline Earth Compounds* (Elsevier, 2013), Chapter 6.
10. U. Rodehorst, M. A. Carpenter, S. Marion, and C. M. Henderson, "Structural phase transitions and mixing behaviour of the Ba-aluminate ($BaAl_2O_4$)-Sr-aluminate ($SrAl_2O_4$) solid solution," Mineral. Mag. **67**(5), 989–1013 (2003).
11. S. Kawaguchi, Y. Ishii, E. Tanaka, H. Tsukasaki, Y. Kubota, and S. Mori, "Giant thermal vibrations in the framework compounds $Ba_{1-x}Sr_xAl_2O_4$," Phys. Rev. B **94**(5), 054117 (2016).
12. E. Tanaka, Y. Ishii, H. Tsukasaki, S. Mori, M. Osada, H. Taniguchi, Y. Sato, and Y. Kubota, "Structural changes and microstructures of $Ba_{1-x}Sr_xAl_2O_4$ for $0 < x < 0.4$," J. Korean Phys. Soc. **66**(9), 1355–1358 (2015).
13. M. V. d. S. Rezende, A. B. Andrade, M. E. G. Valerio, and P. J. R. Montes, "The effect of the host composition on the lifetime decay properties of barium/strontium aluminates compounds," J. Appl. Phys. **115**(10), 103510 (2014).
14. G. Blasse and A. Bril, "Fluorescence of Eu^{2+}-activated alkaline-earth aluminates," Philips Res. Rep. **23**, 201–206 (1968).
15. S. H. M. Poort, W. P. Blokpoel, and G. Blasse, "Luminescence of Eu^{2+} in Barium and Strontium Aluminate and Gallate," Chem. Mater. **7**(8), 1547–1551 (1995).
16. H. Ryu, B. K. Singh, and K. S. Bartwal, "Effect of Sr substitution on photoluminescent properties of $BaAl_2O_4:Eu^{2+}$, Dy^{3+}," Phys. B **403**(1), 126–130 (2008).
17. Q. Xie, B. Li, X. He, M. Zhang, Y. Chen, and Q. Zeng, "Correlation of structure, Tunable Colors, and Lifetimes of (Sr, Ca, Ba)$Al_2O_4:Eu^{2+}$, Dy^{3+} Phosphors," Materials **10**(10), 1198–1210 (2017).
18. J. Botterman, J. Joos, and P. F. Smet, "Trapping and detrapping in $SrAl_2O_4$:Eu,Dy persistent phosphors: Influence of excitation wavelength and temperature," Phys. Rev. B: Condens. Matter Mater. Phys. **90**(8), 085147 (2014).
19. J. Ueda, T. Nakanishi, Y. Katayama, and S. Tanabe, "Optical and optoelectronic analysis of persistent luminescence in Eu^{2+}-Dy^{3+} codoped $SrAl_2O_4$ ceramic phosphor," Phys. Status Solidi C **9**(12), 2322–2325 (2012).
20. D. den Engelsen, P. G. Harris, T. G. Ireland, G. Fern, and J. Silver, "Symmetry-related transitions in the photoluminescence and cathodoluminescence spectra of nanosized cubic $Y_2O_3:Tb^{3+}$," ECS J. Solid State Sci. Technol. **4**(12), R145–R152 (2015).
21. D. den Engelsen, P. G. Harris, T. G. Ireland, G. Fern, and J. Silver, "Symmetry-Related Transitions in the Spectrum of Nanosized Cubic $Y_2O_3:Tb^{3+}$," ECS J. Solid State Sci. Technol. **4**(7), R105–R113 (2015).
22. D. den Engelsen, G. R. Fern, T. G. Ireland, and J. Silver, "Reassignment of electronic transitions in the laser-activated spectrum of nanocrystalline $Y_2O_3:Er^{3+}$," J. Lumin. **196**, 337–346 (2018).